Turbulent Energization of Electron Power Law Tails during Magnetic Reconnection

Giovanni Lapenta●

Department of Mathematics, KU Leuven, Leuven, Belgium and Space Science Institute, Boulder, Colorado, USA

Jean Berchem and Mostafa El Alaoui

Department of Physics and Astronomy, University of California, Los Angeles, California 90095-1547, USA

Raymond Walker●

Department of Earth, Planetary, and Space Sciences, University of California, Los Angeles, California 90095-1567, USA

Earth's magnetotail is an excellent laboratory to study the interplay of reconnection and turbulence in determining electron energization. The process of formation of a power law tail during turbulent reconnection is a documented fact still in need of a comprehensive explanation. We conduct a massively parallel, particle in cell 3D simulation and use enhanced statistical resolution of the high energy range of the particle velocities to study how reconnection creates the conditions for the tail to be formed. The process is not direct acceleration by the coherent, laminar reconnection-generated electric field. Rather, reconnection causes turbulent outflows where energy exchange is dominated by a highly non-Gaussian distribution of fluctuations. Electron energization is diffuse throughout the entire reconnection outflow, but it is heightened by regions of intensified magnetic field such as dipolarization fronts traveling toward Earth.

A ubiquitous feature of space plasmas still defying comprehension is the presence of power law distributed tails of high energy particles [1]. Power law tails occur in heliospheric plasmas and cosmic rays, but we focus here on the magnetosphere surrounding Earth. Observations from the Magnetospheric Multiscale mission [2], like some of its predecessors, show three concurrent features: the presence of reconnection-generated high speed flows, the presence of turbulence within these flows, and the presence of a population of high energy electrons within these turbulent flows [3]. What is the overall mechanism interlinking these three observed processes? Previous studies have already highlighted the link between reconnection outflows and turbulence: Eastwood *et al.* [4] reported greatly heightened electric and magnetic fluctuation spectra with a power law distribution changing slope at hybrid scales that is characteristic of turbulence. Three-dimensional reconnection simulations show this correctly [5,6]. Similarly, there is evidence of a link between particle acceleration and reconnection [7]. Turbulence is one of the oldest mechanisms proposed for particle energization [8]. Significant work has been done in the past few years regarding electron energization in magnetic reconnection [9–12] and in turbulence [13–15]. Recently, Comisso and Sironi [16] investigated the relationship of the two processes in the case of magnetically dominated relativistic plasmas. For the case of the classical plasmas of the heliosphere, the question is still open and of particular relevance to

ongoing missions that are observing high energy particles in the magnetosphere [17] and in the solar wind [18,19].

To answer this question, we use a combined approach where we first conduct a global magnetohydrodynamic (MHD) magnetosphere simulation to provide the global forcing for reconnection as well as the general environment where the reconnection outflow jet forms and interacts with its surroundings. When reconnection is already active, we select the region of interest encompassing the whole outflow jet and launch a fully kinetic particle in cell (PIC) simulation that can study with accuracy the electron and ion motion, resolving directly the mechanisms of particle acceleration. Previous work [20,21] shows the ability of PIC to introduce the correct physics of reconnection when started from a MHD state that misses important physics. After a short transient, the electrons become decoupled from the ions and produce the typical signature of kinetic reconnection [20,22], forming much faster jets that carry substantial energy [23,24]. Also, a number of instabilities due to the kinetic physics develops [25]. Details of the model are given in Walker *et al.* [25].

The PIC method has limited ability to resolve the particle energy distribution. Most PIC methods apply the Box-Müller algorithm [26] to generate a drifting Maxwellian distribution with particles of equal weight. In this approach, very few particles are generated in the tail at high speed and the vast majority have speeds close to the drift. This statistical limitation leads to the inability of PIC to capture phenomena acting primarily on the tail. Byers [27] (see also

Chap. 17 in Birdsall and Langdon [28]) showed that a different loading biased toward more higher energy particles, but with correspondingly reduced statistical weight, leads to a much improved description of the interaction of waves with the tail of the distribution (e.g., Landau damping).

To remove this limitation, we use two species each for electrons and ions. One species is the core bulk population of thermal particles; and the second species, with reduced statistical weight, represents the power law tail. This approach differs from a test particle approach [12], in that even the smaller weight particles still contribute to the overall energy budget. This is an important difference because our treatment still conserves energy, and the energy needed to accelerate the particles comes from the fields. As an alternative, the importance sampling method [27,29] can be used to generate uniformly distributed particles in velocity space with weights corrected to represent a Maxwellian: this approach leads to results consistent with those reported here [30].

In this Letter, using this approach, we reach two conclusions. First, the core population receives modest energization but the energy of the power law electrons increases dramatically, explaining the observed prevalence of high energy particles in reconnection outflows. Second, the mechanism of particle acceleration for the high speed tail is not directly linked with reconnection. Instead, the acceleration comes from the interaction of the particles with the high-speed reconnection outflow that forms fronts of increased magnetic field (called dipolarization fronts when traveling earthward) and leads to the production of a turbulent cascade. We observe a net energization of the particles: especially in the regions of fastest flows and largest vertical field intensification.

We start our study with a generic global MHD model of Earth in geocentric solar magnetospheric (GSM) coordinates that assumes a constant solar wind flow with an earthward speed of $V_x = -530$ km/s, a density of $n = 6$ cm^{-3}, a thermal pressure of $p = 180$ pPa, and a southward directed interplanetary field of $B_z = -8$ nT. We observe reconnection developing on the night side of the magnetosphere, in the magnetotail [30]. We consider this reconnecting tail as the initial condition for a PIC simulation that includes the subdomain: $x/R_E = [-38.2, -7]$, $y/R_E = [-7.8, 7.8]$, and $z/R_E = [-10.4, 10.4]$ using the MHD simulation results for initial and boundary conditions. The PIC simulation uses $400 \times 200 \times 280$ cells with 125 particles per cell per species, arranged in a topology of $40 \times 10 \times 14$ processors. The time step is $\omega_{\mathrm{pi}} \Delta t = 0.5$, where the reference density used for computing the plasma frequency is $n_0 = 0.25$ cm^{-3}. The size of Earth is $R_E/d_{p0} = 14.0$, and the duration of the simulation (8000 cycles) corresponds to about 30 s of real time.

We derive the initial state of the PIC simulation from an MHD state by making the assumption that the distribution is Maxwellian, with the density from MHD and species velocities determined from the bulk speed and the MHD

current density. We assume the MHD temperature is that of the ions, while the electron temperature is 5 times smaller, as is typical in the magnetotail.

As mentioned above, we use two main species (0 for the electrons and 1 for the ions) for the core bulk population of thermal particles and capture the low probability tail distribution by using two additional species (2 for the electrons and 3 for the ions) distributed initially with a power law tail. We achieve this by sampling the tail of a kappa distribution [31], with $\kappa = 2$, using the modified Box-Müller [26] transform algorithm described in Ref. [32], with the condition $v > v_{\mathrm{th},s}$. The statistical weight of the tail particles was 10^{-3} of the weight of the bulk species to extend the dynamical range by 3 orders of magnitude. This is an arbitrary choice, but using a more neutral importance sampling method does not lead to different conclusions, as shown in the Supplemental Material [30].

The top panel of Fig. 1 presents evolution of the energy fluxes for the electron species starting at the beginning for
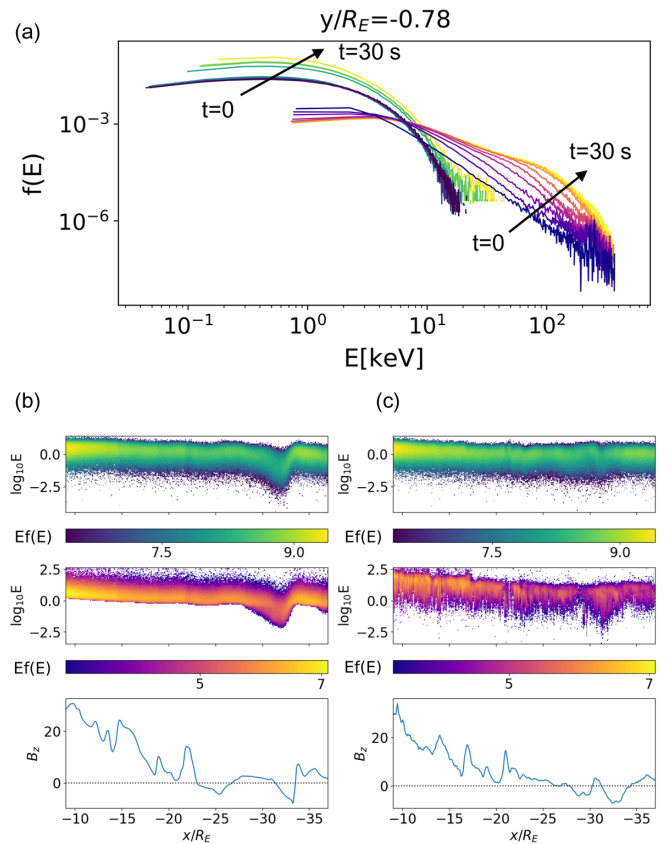

FIG. 1. Temporal evolution of the energy distribution: (a) evolution of the particle distribution function for species 0 (bulk electrons) and species 2 (tail electrons) during the evolution from a time of 0 s to a time of 30 s in nine equally spaced linear steps in time (darker to lighter); and (b) and (c) reports of energy fluxes $Ef(E)$ of species 0 and species 2 stacked with the vertical magnetic field B_z, at the initial and final times. Distribution is taken for a narrow band of $y = Ly/2 \pm d_i/2$ and $z = Lz/2 \pm d_i/2$.
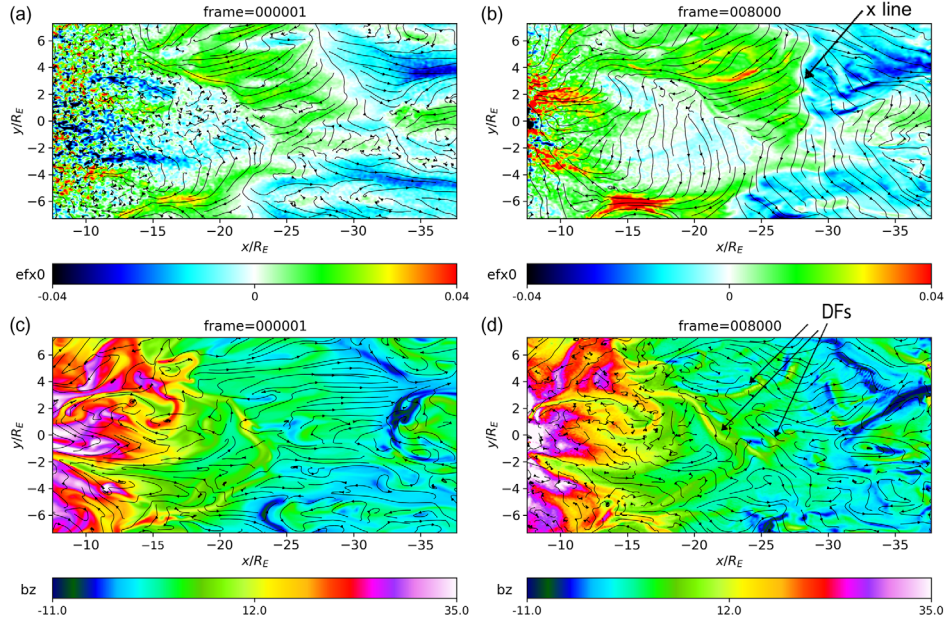
FIG. 2. Temporal evolution of the bulk electron energy flux [top; (a) and (b)] and of the vertical component of the magnetic field [bottom; (c) and (d)]. Black lines show, in top panels, the bulk Maxwellian electron speed (species 0) on the equatorial plane and, in bottom panels, the magnetic field on the equatorial plane. The initial (left) and final (right) times are shown. Arrows point to the location of the so-called x line, the center of reconnection, and a few dipolarization fronts (DFs) identified by areas of larger vertical field B_z.

the PIC simulation. The primary conclusion is that the power-law tail electrons are indeed energized much more than the bulk electrons. In particular, Fig. 1(a) shows the electron energy distribution for both species of electrons at the beginning and at different times during the simulation. As can be observed, a power law tail forms, extending to high energies. The bulk electrons do not change their distribution by as much. This is consistent with the results from PIC simulations without the high energy tail.

Figures 1(b) and 1(c) show the change in the energy fluxes of electrons in species 0 (bulk) and 2 (power law tail) from the initial to the final times. There is a striking difference between bulk and kappa tail electrons. For the bulk Maxwellian electrons, energization is present but weak. For the tail kappa-distributed electrons, energization is by a full order of magnitude everywhere but larger in the near-Earth region. By the end of the simulation, energization is starting to saturate. Attentive inspection reveals that the higher energy particles have a tendency to concentrate in correspondence with the intensification of the vertical component of the magnetic field B_z.

It is worth noting that in an identical simulation without the additional tail species, no significant power law tails formed. Conversely, using importance sampling of a Maxwellian plasma with no initial power law tail leads to substantially similar acceleration of the high energy tail to that reported in Fig. 1 [30]: there is no need to seed a power law initially to obtain one as part of the energization process.

This is our central result: the electric fields generated in the reconnection process do not significantly affect the

energy spectrum at low energies but greatly increase the high energy tail, as is well known from observations (e.g., Ref. [3]). The novelty here is the ability to replicate the process *in silico*: a fact that allows us to investigate correlations between quantities in space and time in a manner not possible from spacecraft observations.

Figure 2 shows the evolution of the system in the equatorial maximum pressure plane. The tail current sheet does not remain perfectly flat as a function of time and develops some warping. We use GSM coordinates (x is toward the Sun, y is in the dawn to dusk direction, and z is in the northward direction) and project the information on a flat visualization plane defined for each position (x, y) by the location in z where the trace of the ion pressure tensor is maximum.

The reconnection location can be clearly identified by considering the electron energy flux along x (see arrow in Fig. 2). This flux is defined as the third-order moment of the distribution function of the velocity of the particles for each species s, $\mathcal{E}_{xs} = \int v_x m_s v^2 f(\mathbf{v}) d\mathbf{v}/2$. The position of the x line can be identified as the narrow white band, roughly located in $x \in [-30, -20] R_E$ between the positive (green) and the negative (cyan) electron energy fluxes. This is the condition at the x line where the energy flux is earthward on the Earth side and tailward on the tail side. The inappropriately called x line is very far from being the straight line assumed in the common analytical models that impose periodic boundary conditions in the dawn-dusk direction y.

In the two reconnection outflow regions, the vertical component of the magnetic field has considerable structure
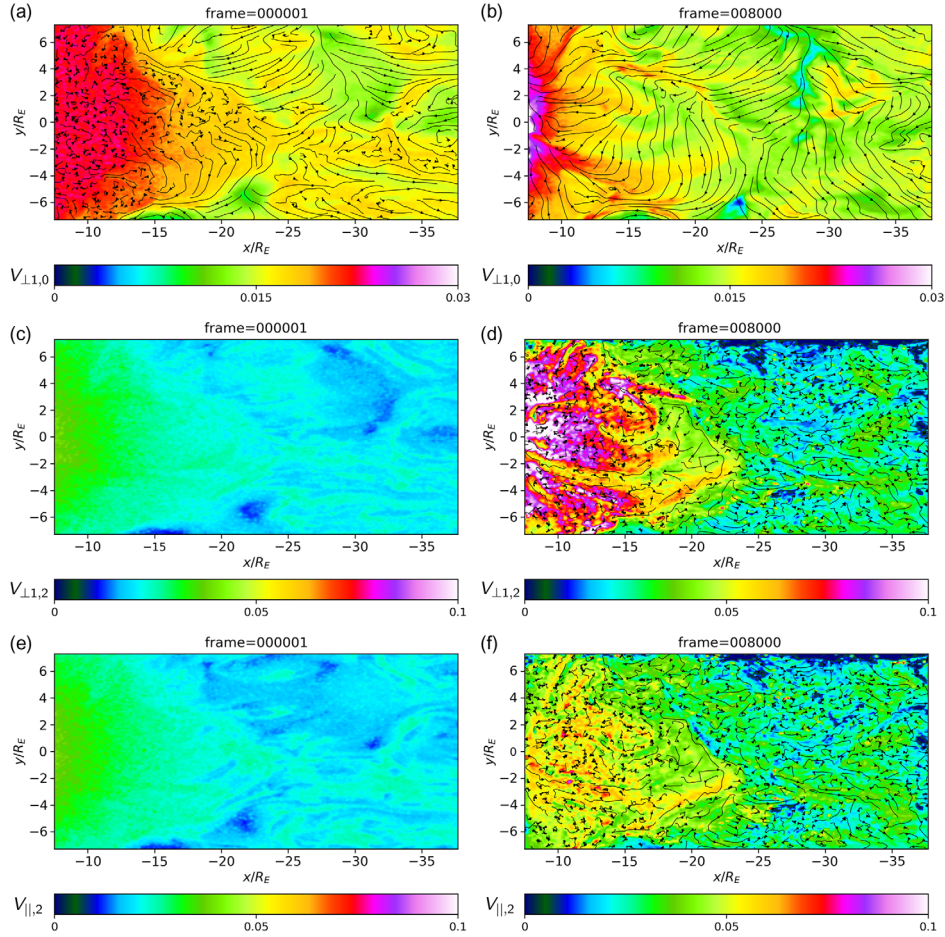
FIG. 3. Temporal evolution of the thermal speed (normalized to the speed of light) defined from the second moment of the electron velocity distribution. Two species are shown: the bulk Maxwellian electrons [species 0, top; (a) and (b)] and the kappa-distributed electrons [species 2, perpendicular in the middle; (c) and (d) and parallel on the bottom; (e) and (f)]. The black lines show the flow field on the equatorial plane for both electron species (initially, there is no flow for species 2). The kappa electrons are much more turbulent than the bulk electrons.

(right panels in Fig. 2). These are fronts of magnetic energy traveling earthward on the earthward side (called dipolarization fronts) or tailward on the tailward side.

The temperature of the kappa tail increases by an order of magnitude in vast regions of the simulation domain; see Fig. 3. The process of energization is nonuniform. The region near the x line cools while the heating strongly correlates with the regions of intensified vertical magnetic field (both positive and negative). This effect is especially strong for the kappa tail electrons. One can follow the complicated structure in the earthward region to the left of $x = -25R_E$; the same features are seen in B_z and in $v_{\mathrm{th},2,\perp}$.

The process of heating for all species is highly anisotropic. However, it remains fairly gyrotropic, except for the region of the x line itself where gyrotropy is broken. Comparing the middle and bottom rows of Fig. 3, it is evident that the heating is predominant in the perpendicular direction. Overall, the heating is clearly not laminar.

Next, we investigate the fluctuations of the conversion rate of electromagnetic energy into particle energy, $\mathbf{J}_s \cdot \mathbf{E}$,

as a function of the earthward ion flow V_{ix} and the vertical component of the magnetic field B_z. The former is a proxy for the distance away from the reconnection x line as the reconnection outflow speed increases away from the reconnection site that is a stagnation point.

Figure 4 shows the results of this conditional fluctuation analysis for the power law electrons, species 2. The energization has a wide range of fluctuations at all distances from the x line (indicated by V_{ix}). The turbulence is intermittent. This is determined both by visual inspection and by noticing the non-Gaussian aspect of the fluctuation spectrum [i.e., nonparabolic in Fig. 4(c)], which is known to be a good indicator of intermittency [33].

Taking the mean and the standard deviation of the distribution of fluctuations, we observe that there is a net energization for velocities between 0 and positive 200 km/s, the region of the earthward outflow, and for the positive vertical component of B_z. But, this net heating comes as an average of a highly turbulent spectrum of fluctuations where the standard deviation largely exceeds
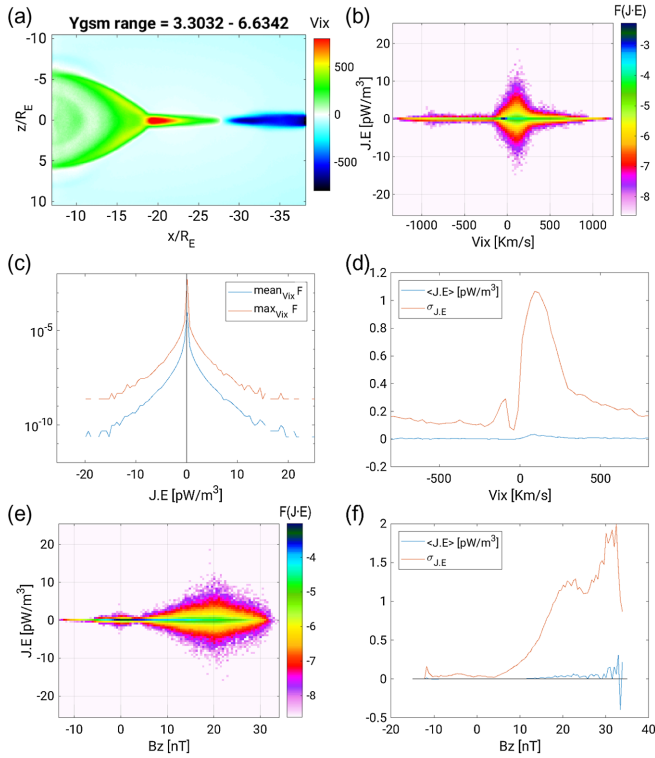
FIG. 4. Conditional bivariate analysis of the fluctuations of the energy exchange for electron species 2 (kappa tail), $\mathbf{J}_2 \cdot \mathbf{E}$, as a function of V_{ix} and B_z at cycle 1000, corresponding to $t = 3.75$ s, considering the range $y = [3.3, 6.6] R_E$: (a) false color representation of V_{ix}, averaged over y in the range indicated; (b) conditional fluctuation spectrum (measured as $\log_{10}$ of fraction F of points in the grid) at different V_{ix}, integrated over B_z, showing the dominance of positive transfer (i.e., toward the particles) over negative (i.e., toward the field); (c) mean and maximum (along V_{ix}) values of the distribution of fluctuations $\mathbf{J}_2 \cdot \mathbf{E}$, showing that the positive side dominates over the negative side and showing a clear nonparabolic shape, indicative of intermittency; and (d) mean and standard deviation of $\mathbf{J}_2 \cdot \mathbf{E}$ as a function of V_{ix}. This clearly shows energization for positive V_{ix} between 0 and 200 km/s [regions that can be identified as green in Fig. 4(a)], meaning that in the earthward flow, turbulence deposits more energy on average than it takes away. Figure 4(e) gives the conditional fluctuation spectrum of $\mathbf{J}_2 \cdot \mathbf{E}$ at different B_z, integrated over V_{ix}, indicating that energy exchange is concentrated in regions of positive normal field, peaking at around 20 nT; and Fig. 4(f) gives the mean and standard deviation of $\mathbf{J}_2 \cdot \mathbf{E}$ as a function of B_z, showing that at positive normal fields, the energy exchange has a net positive value causing electron energization.

the mean value. We conclude that the energization is then caused by the turbulent cascade of energy concentrated in the earthward regions of larger vertical fields. This finding is consistent with adiabatic acceleration [30,34–36].

In summary, we have shown that, by using a combined MHD and PIC analysis, where one electron-ion population of computational particles describes the bulk and a second the high energy tail, we can replicate the observed formation of a high energy power law tail during reconnection in Earth's magnetotail. In contrast to observations that are local and instantaneous, the simulation provides us a global view of the temporal evolution that allows us to investigate the mechanisms of energization by using statistical methods. We find that there is a strong energization in the earthward outflow from reconnection and, within it, especially in the regions of the intensified vertical field. The mechanism of energy transfer that forms the power law tail is characterized by highly fluctuating energy exchanges, with the standard deviation largely exceeding the mean.

While the study reported here focuses on the conditions observed in Earth's magnetotail, the mechanisms described are based on the fundamental properties of turbulence and reconnection; and it can be expected that similar processes might be present in all instances in laboratory or natural plasmas where reconnection outflows develop turbulence.

[1] I. Zouganelis, J. Geophys. Res. **113**, A08111 (2008).
[2] J. Burch, R. Torbert, T. Phan, L.-J. Chen, T. Moore, R. Ergun, J. Eastwood, D. Gershman, P. Cassak, M. Argall et al., Science **352**, aaf2939 (2016).
[3] M. Øieroset, R. P. Lin, T. D. Phan, D. E. Larson, S. D. Bale, and A. Szabo, Phys. Rev. Lett. **89**, 195001 (2002).
[4] J. P. Eastwood, T. D. Phan, S. D. Bale, and A. Tjulin, Phys. Rev. Lett. **102**, 035001 (2009).
[5] F. Pucci, S. Servidio, L. Sorriso-Valvo, V. Olshevsky, W. Matthaeus, F. Malara, M. Goldman, D. Newman, and G. Lapenta, Astrophys. J. **841**, 60 (2017).
[6] F. Pucci, W. H. Matthaeus, A. Chasapis, S. Servidio, L. Sorriso-Valvo, V. Olshevsky, D. Newman, M. Goldman, and G. Lapenta, Astrophys. J. **867**, 10 (2018).
[7] M. Øieroset, R. P. Lin, T. D. Phan, D. E. Larson, S. D. Bale, and A. Szabo, Phys. Rev. Lett. **89**, 195001 (2002).
[8] E. Fermi, Phys. Rev. **75**, 1169 (1949).
[9] J. Dahlin, J. Drake, and M. Swisdak, Phys. Plasmas **21**, 092304 (2014).
[10] J. Dahlin, J. Drake, and M. Swisdak, Phys. Plasmas **22**, 100704 (2015).

[11] J. Dahlin, J. Drake, and M. Swisdak, Phys. Plasmas **24,** 092110 (2017).

[12] M. Zhou, M. El-Alaoui, G. Lapenta, J. Berchem, R. L. Richard, D. Schriver, and R. J. Walker, J. Geophys. Res. **123,** 8087 (2018).

[13] V. Zhdankin, D. A. Uzdensky, G. R. Werner, and M. C. Begelman, Phys. Rev. Lett. **122,** 055101 (2019).

[14] V. Zhdankin, D. A. Uzdensky, G. R. Werner, and M. C. Begelman, Mon. Not. R. Astron. Soc. **493,** 603 (2020).

[15] A. Lazarian, G. Kowal, S. Xu, and A. Jafari, J. Phys. **1332,** 012009 (2019).

[16] L. Comisso and L. Sironi, Astrophys. J. **886,** 122 (2019).

[17] R. Torbert, J. Burch, T. Phan, M. Hesse, M. Argall, J. Shuster, R. Ergun, L. Alm, R. Nakamura, K. Genestreti *et al.*, Science **362,** 1391 (2018).

[18] R. Chhiber, A. V. Usmanov, W. H. Matthaeus, T. N. Parashar, and M. L. Goldstein, Astrophys. J. Suppl. Ser. **242,** 12 (2019).

[19] D. Mueller, R. G. Marsden, O. S. Cyr, H. R. Gilbert, Sol. Phys. **285,** 25 (2013).

[20] M. Ashour-Abdalla, G. Lapenta, R. J. Walker, M. El-Alaoui, and H. Liang, J. Geophys. Res. **120,** 4784 (2015).

[21] G. Lapenta, J. Berchem, M. Zhou, R. Walker, M. El-Alaoui, M. Goldstein, W. Paterson, B. Giles, C. Pollock, C. Russell *et al.*, J. Geophys. Res. **122,** 2024 (2017).

[22] M. Ashour-Abdalla, G. Lapenta, R. Walker, M. El-Alaoui, H. Liang, M. Zhou, J. Berchem, and M. L. Goldstein, Geophys. Res. Lett. **43,** 6005 (2016).

[23] G. Lapenta, M. Ashour-Abdalla, R. J. Walker, and M. El Alaoui, Geophys. Res. Lett. **43,** 515 (2016).

[24] G. Lapenta, M. El Alaoui, J. Berchem, and R. Walker, J. Geophys. Res. **125,** e2019JA027276 (2020).

[25] R. J. Walker, G. Lapenta, J. Berchem, M. El-Alaoui, and D. Schriver, J. Plasma Phys. **85,** 905850109 (2019).

[26] G. E. Box and M. Müller, Ann. Math. Stat. **29,** 610 (1958).

[27] J. Byers, Noise suppression techniques in macroparticle models of collisionless plasmas, Technical Report No. N32830, California University, Livermore, Lawrence Radiation Lab., 1970.

[28] C. Birdsall and A. Langdon, *Plasma Physics Via Computer Simulation* (Taylor & Francis, London, 2004).

[29] R. Y. Rubinstein and D. P. Kroese, *Simulation and the Monte Carlo Method*, Vol. 10 (John Wiley & Sons, New York, 2016).

[30] See Supplemental Material at http://link.aps.org/supplemental/10.1103/PhysRevLett.125.225101 for a comparison of the results obtained with 2 particle population per species versus importance sampling, as well as for a movie of the 3D volume rendering of the ion current at the end of the simulation (cycle 8000) with magnetic field lines selected progressively closer to the viewer.

[31] V. Pierrard and M. Lazar, Sol. Phys. **267,** 153 (2010).

[32] R. Abdul and R. Mace, Comput. Phys. Commun. **185,** 2383 (2014).

[33] E. Marsch and C. Tu, Ann. Geophys. **12,** 1127 (1994).

[34] Q. Pan, M. Ashour-Abdalla, M. El-Alaoui, R. J. Walker, and M. L. Goldstein, J. Geophys. Res. **117** (2012).

[35] M. Akhavan-Tafti, J. Slavin, W. Sun, G. Le, and D. Gershman, Geophys. Res. Lett. **46,** 12654 (2019).

[36] J. Egedal, W. Daughton, and A. Le, Nat. Phys. **8,** 321 (2012).